INTER-RELATIONS BETWEEN INTRASEASONAL AND INTERANNUAL RAINFALL VARIABILITY IN TROPICS

Yimin Ji
School of Computational Sciences, George Mason University, Fairfax, VA 22030, USA

1. INTRODUCTION

The tropical rainfall exhibits quasi-regular low frequency variability on both interannual and intraseasonal time scales. However, many aspects of the interrelationship between intraseasonal and interannual modes especially the linkage between Madden-Julian Oscillation (MJO, Madden and Julian 1994) and ENSO have not been described and understood clearly. Specifically, whether ENSO and MJO modulate or alter each other are still controversial (Slingo et al 1999; Kessler and Kleeman 2000). This paper examines the interannual and intraseasonal variability of tropical rainfall and physical linkages between them.

2. RAINFALL VARIATIONS DURING 1979-2002

The rainfall data used in this section is the Global Precipitation Climatology Project (GPCP, Janowiak and Arkin 1991) pentad data that started in 1979. Sea surface temperature (SST) is from AVHRR weekly product. The mean DJFM rainfall and rain variance during 1979-2002 (Fig. 1) indicated largest variance around the date line to the south of equator as well as in Indian Ocean ITCZ corresponding to the large mean rainfall in these regions. The rain variance in summer (Fig. 2) is dominated by summer monsoon and east Pacific ITCZ.

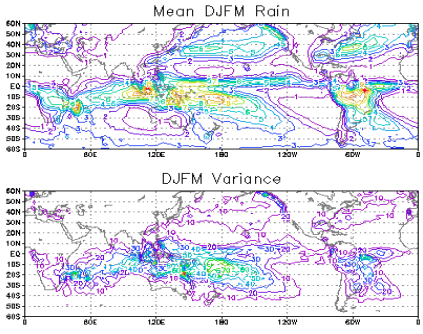

Fig.1 Mean DJFM rainfall rate (upper) and variance (lower) during 1979-2002

The time series of pentad were filtered using a 30-60 day band pass filter. The hovannval(time-longitude) variability during the 23 years period (Fig. 3) shows the effect of ENSO cycle on modulating the MJO. The ENSO seems affecting both eastern and western envelope. The eastern envelop intensifies during cold episode and the western envelop intensifies in the warm episode. However, the most evident linkage is that the eastern envelope stretches beyond the date line during the ENSO warm phase. At decadal scale, the western envelop shows an eastward shifting since the beginning of 90's.

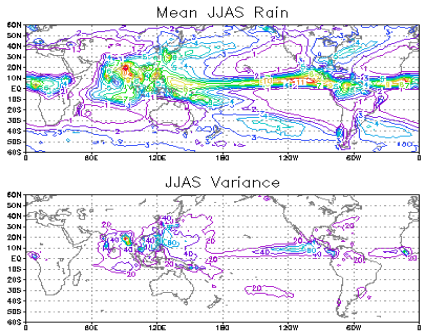

Fig.2 Mean JJAS rainfall rate (upper) and variance (lower) during 1979-2002

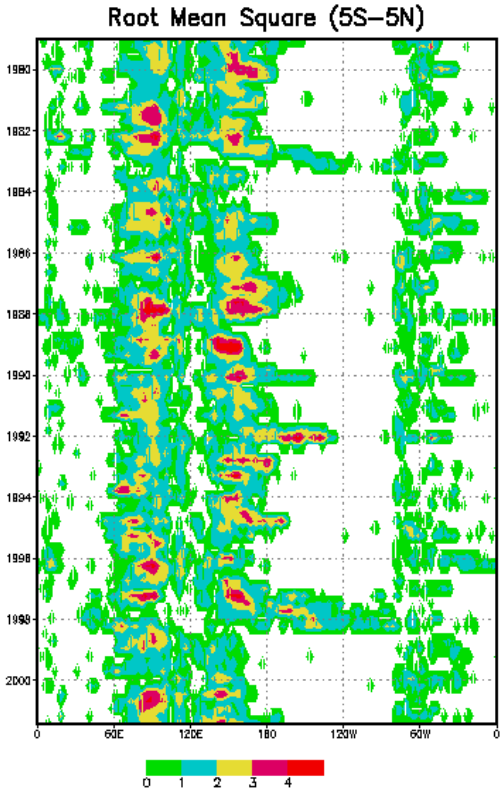

Fig.3 Hovannval root mean square variability during 1979-2002 for 30-60 day band passed rainfall

3. EXTENDED EOF AND SSA METHODS

EOF is one of the most commonly used techniques to extract qualitative information from two dimensional (temporal and spatial) data in atmospheric science (e.g. Lorenz, 1956; Barnett, 1977). The EOF method involves the solution of the eigenvector equation:

$$(\mathbf{R} - \mu\mathbf{I})\mathbf{e}_m = 0 \qquad (1)$$

where $\mathbf{R}=\mathbf{F}\mathbf{F}^T/\mathbf{N}$ is the data covariance matrix, **F** is a matrix with M rows and N columns. M is the dimension of the spatial field and N is the temporal dimension or number of instantaneous samples. **I** is a unit matrix, μ is eigenvalue and $\mathbf{e}_m$ is the resulting eigenvector (EV), and m = 1, 2, …, M. Each of the eigenvalues explains a fraction of total variance and leads to an eigenvector solution that describes one mode of the spatial variability. The temporal behavior of data associated with the EV mode is represented by the principal components (PC) that are coefficients in reconstructing the data in eigenvector space. The detail of the notion of EOF can be found in Broomhead and King (1986). In normal cases, the dimension of the temporal vector (N) should be larger than the dimension of the spatial vector (M) to generate a normal covariance matrix **R**(M, M). This often limits the resolution of the spatial data.

Extended EOF (EEOF) follows the similar derivation of EOF. However, the resulting eigenvector is required to be linear predictors of a data field not only at a given time but also at some successive times. Therefore, EEOF show not only eigenvector patterns but also temporal evolutions of eigenvectors. Technically, EEOF build the data matrix **F** with M*L rows and N-L+1 columns for the data set described in above EOF analysis. Where L is number of time lags. Therefore, EEOF generate a much bigger covariance matrix and therefore require significantly more computer resources. EEOF also require longer time series of the data. This paper uses EEOF to identify temporal sequence of spatial variations and the associated temporal spectrum.

The SSA has been developed and used in atmospheric science quite recently (Vautars and Gil, 1989; Rasmusson et al., 1990). Although the SSA involves the solution of the same eigenvector equation, it address the spectrum aspect of the chaotic data instead of the spatial patterns in EOF. The data used in SSA is a one dimensional time series. In SSA, the **R** in equation (1) is an auto-correlation matrix of the time series. The size of the auto-correlation matrix of the times series is determined by the number of lags (M). Normally, the number of lags must be at least an order of magnitude smaller than the size of the time series. This requires time period of data be much longer than the spectrum of interest. In this study, the SSA is used to capture the intra-seasonal spectrum, the number of lags is about 20 (100 days) that is an order smaller than the length of the time series (four years). The eigenvectors of SSA capture the spectrum of the time series, while the principal components show the temporal behavior of the spectrum. Therefore, the EEOF method was applied to the time series of global data, while the SSA was applied to time series in regions of interest.

The first EEOF, which explains 7% of the total variances, from DJFM analysis (Fig. 4) indicate a stationary pattern. The centers of the dipole are located at 130° E and 170° W. The patterns do not vary during a 55-day sequence.

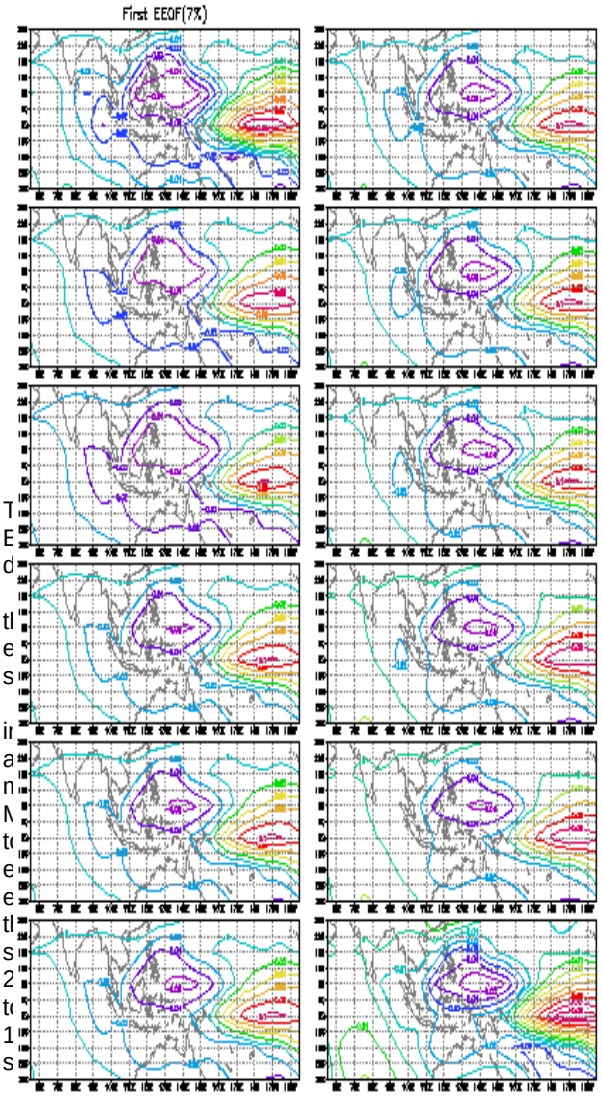

Fig. 4 First EEOF from DJFM rainfall data, each successive lag is 5 days.

The second EEOF (Fig. 5) represents a transit patter. The centers of the dipole are located at 90° E and 170° E. The dipole completes a total oscillation within 60 days with a phase speed about 3.5 m/s.

The PCs of the first two EEOF (Fig. 6) indicate that the first EEOF is more linked to the ENSO signal and explains less variance of MJO as compared to the second EEOF.

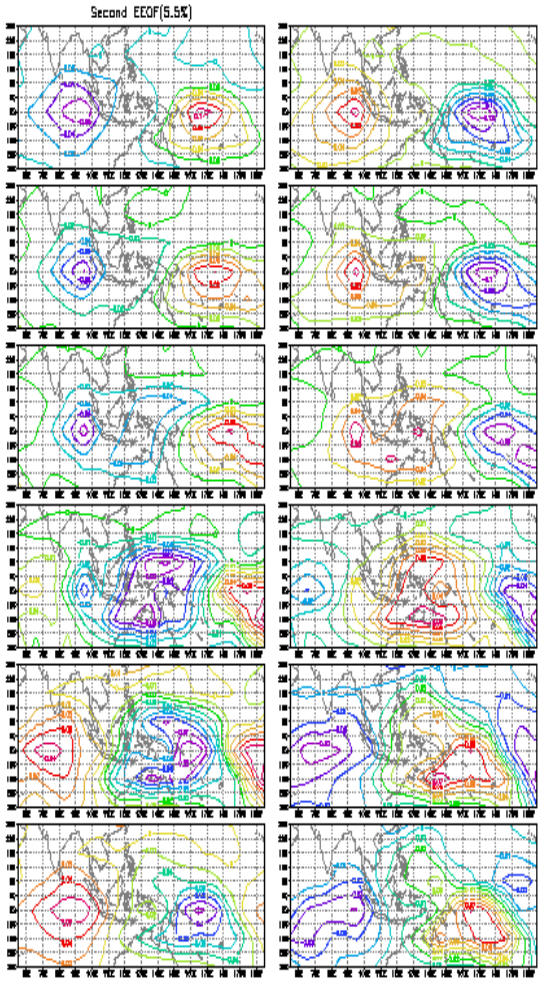

Fig. 5 Second EEOF from DJFM rainfall data, successive lag is 5 days.

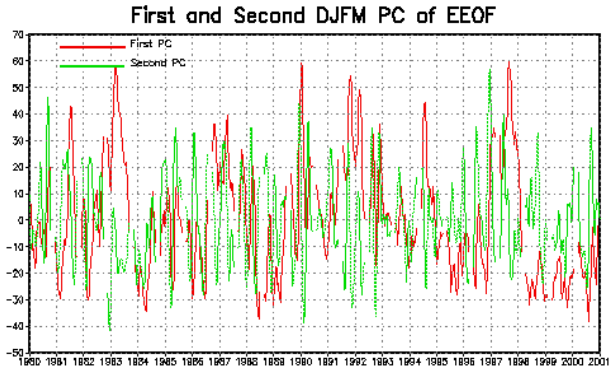

Fig. 6 PCs of the first two EEOF

The SSA eigenvector of the first PC of EEOF (Fig. 7) indicates a dominant model of interannual variability associated with ENSO cycle. The first (mean) modes explains about 63% of the total variance. The MJO mode (third and fourth) explains about 16% of the total variance. The 25-30 day mode (fifth to seventh) explains about 3% of the variance.

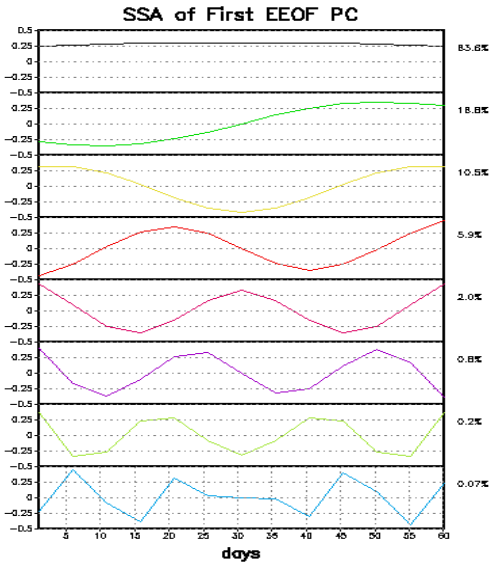

Fig. 7 First 8 eigenvectors of SSA derived from the PC of the first EEOF from DJFM rainfall data

The SSA eigenvector of second PC of EEOF (Fig. 8) represents the dominant mode of MJO. The MJO mode (first and second) explains about 73% of the total variance. The 25-30 day mode (fourth and fifth) explains 11% of the total variance. The mean mode (third) explains only 15.9% of the variance and is weakly linked to ENSO signal

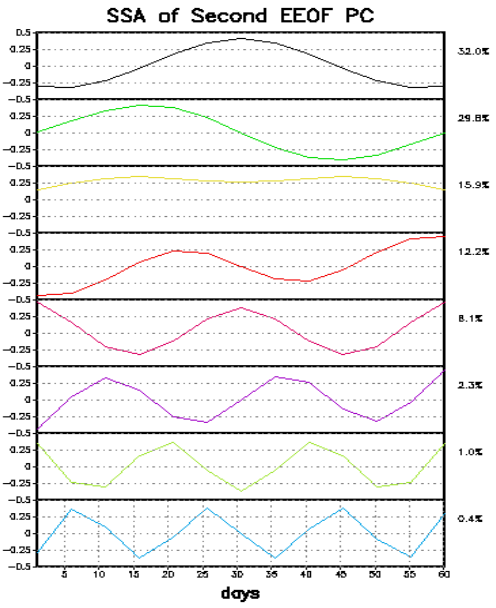

Fig. 8 First 8 eigenvectors of SSA derived from the PC of the second EEOF from DJFM rainfall data

4. TRMM-GPCP PARALLEL ANALYSIS

In order to verify the above finding, the TRMM rain product, which provides more reliable estimate, was used to compare the GPCP spectral results. The time series (Fig. 9) indicate that in strong MJO zone, TMI and GPCP rain estimates are very close on both spectrum and magnitude. In weak MJO zone, TMI estimates show stronger oscillation and wet biases.

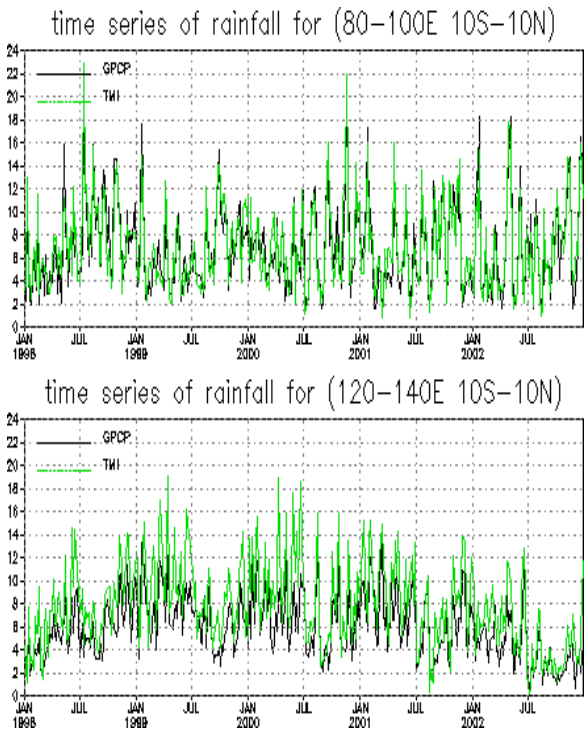

Fig. 9 Time series of GPCP and TMI rain estimates.

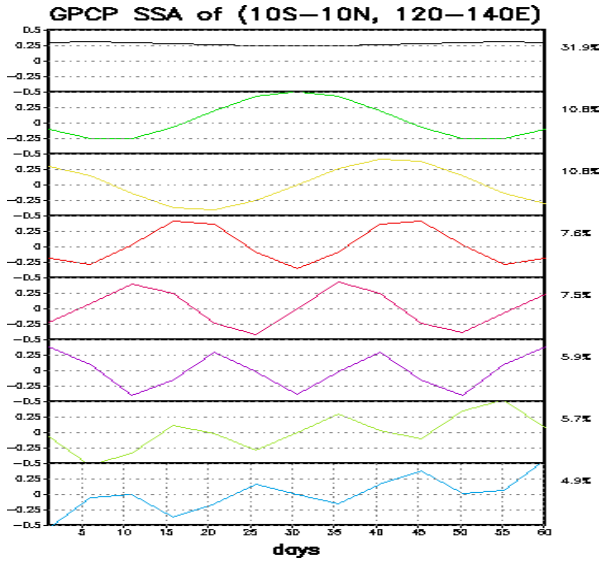

Fig. 10 First 8 eigenvectors of SSA derived from GPCP time series averaged over (10S-10N, 120-140E).

The parallel spectrum analyses for the two data sets show similar patters (Fig. 10, Fig. 11).

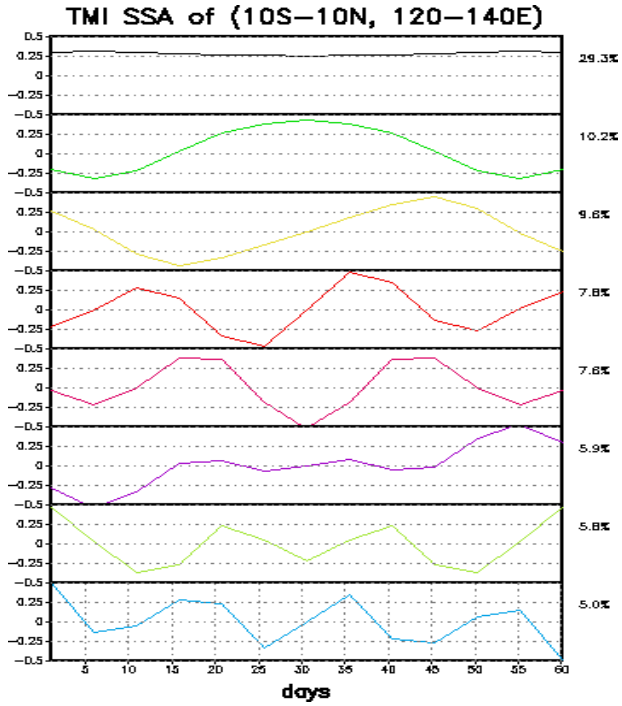

Fig. 11 First 8 eigenvectors of SSA derived from TMI time series averaged over (10S-10N, 120-140E).

Reference

Barnett T. P. (1977) The principal time and space scales of the Pacific trade wind fields. J. Atmos. Sci. 34: 221-236

Broomhead D. S., King G. P. (1986) Extracting qualitative information from experimental data. Physica D 20: 217-236

Janowiak, J. E., and P. A. Arkin, 1991: Rainfall variations in the tropics during 198601989, as estimated from observations of cloud-top temperature. J. Geophys. Res., 96, 3359-3373.

Kessler, W. S., and R. Kleeman, 2000: Rectification of the Madden-Julian Oscillation into the ENSO cycle, J. Climate, 13, 3560-3575.

Lorenz E. N. (1956) Empirical orthogonal functions and statistical weather prediction. Department of Meteorology, MIT Science Report 1: pp 49

Madden RA, Julian PR (1994) Observations of the 40-50-Day Tropical Oscillation- A Review. Mon. Wea. Rev. 122: 814-837

Rasmusson E. M., Wang X., Ropelewski C. F. (1990) The biennial component of ENSO variability. J. Mar. System 1: 71-96

Slingo, J. M>, D. P. Rowell, K. R. Sperber, and F. Nortley, 1999: On the predictability of the interannual behavior of the Madden-Julian oscillation and its relationship with El Nino. Quart. J. Roy. Meteor. Soc., 125, 583-610.

Vautard R, Ghil M (1989) Singular spectrum analysis in nonlinear dynamics, with applications to paleoclimatic time series. Physica D 35: 395-424